Nanoscale

COMMUNICATION

View Article Online
View Journal | View Issue

Cite this: *Nanoscale*, 2018, **10**, 18113

Received 11th July 2018,
Accepted 18th September 2018

DOI: 10.1039/c8nr05598j

rsc.li/nanoscale

Assembly of cellulose nanocrystals in a levitating drop probed by time-resolved small angle X-ray scattering†

Yingxin Liu, [a,b] Michael Agthe,‡[a] Michaela Salajková,[c] Korneliya Gordeyeva,[a] Valentina Guccini,[a,b] Andreas Fall,§[a] Germán Salazar-Alvarez,[a,b] Christina Schütz *¶[a,b] and Lennart Bergström *[a]

Assembly of bio-based nano-sized particles into complex architectures and morphologies is an area of fundamental interest and technical importance. We have investigated the assembly of sulfonated cellulose nanocrystals (CNC) dispersed in a shrinking levitating aqueous drop using time-resolved small angle X-ray scattering (SAXS). Analysis of the scaling of the particle separation distance (*d*) with particle concentration (*c*) was used to follow the transition of CNC dispersions from an isotropic state at 1–2 vol% to a compressed nematic state at particle concentrations above 30 vol%. Comparison with SAXS measurements on CNC dispersions at near equilibrium conditions shows that evaporation-induced assembly of CNC in large levitating drops is comparable to bulk systems. Colloidal states with *d vs. c* scalings intermediate between isotropic dispersions and unidirectional compression of the nematic structure could be related to the biphasic region and gelation of CNC. Nanoscale structural information of CNC assembly up to very high particle concentrations can help to fabricate nanocellulose-based materials by evaporative methods.

Introduction

Assembly of nano-sized building blocks into complex architectures is both a promising route for the fabrication of functional materials and also a design principle in nature.[1–4] With the significant advances during the last decades in tailoring assembled structures and functionalities of synthetic nanoparticles,[5,6] there is a rapidly growing interest to utilise nanoparticles from renewable sources in sustainable materials. However, producing sustainable nanomaterials with tailored and hierarchical structures is challenging and requires better understanding on how to exercise the structural control of assemblies of bio-based nanoparticles.[7,8]

Nanocellulose is a fibrous nanoparticle that can be readily extracted from wood and other sources (*e.g.* cotton, ramie and bacteria).[9] The helical orientation of nanocellulose in plant cell walls has been shown to contribute to both the mechanical strength of wood,[10–12] as well as the brilliant colour of different organisms.[13–15] Rod-like cellulose nanocrystals (CNC) with a high aspect ratio produced by *e.g.*, sulphuric acid hydrolysis are colloidally stable in aqueous dispersions and form a chiral nematic (cholesteric) liquid crystalline phase at relatively low concentrations.[10,16] Drying of CNC dispersions results in films with a helically arranged structure and iridescent optical appearance with potential applications as sensors and coatings.[3,17–19] Studies of the assembly and compression of the chiral nematic structure during film formation are sparse and restricted to relatively low particle concentrations.[20]

The helical assembly (*e.g.*, the chiral nematic pitch) of CNC as a function of the particle concentration has been studied in both bulk phase and in constrained spherical geometries.[16,21–26] However, recent studies on emulsion drops and micro-drops generated by microfluidics were restricted to a relatively narrow concentration range of CNC and were invariably performed on aqueous drops dispersed in organic solvents containing surfactants or surface active copolymers,[21–23] which may have a significant influence on the nucleation of the cholesteric phase.[27]

Acoustic levitation of aqueous drops is a convenient approach which has been used to study the crystallization and agglomeration of proteins as well as the assembly of nanoparticles.[28–30] Levitating drops that slowly shrink as the water evaporates constitute a system that does not require the addition of surfactants and allows assembly to be studied

[a]*Department of Materials and Environmental Chemistry, Stockholm University, 106 91 Stockholm, Sweden. E-mail: christina.schuetz@gmail.com, lennart.bergstrom@mmk.su.se*
[b]*Wallenberg Wood Science Center, KTH, 100 44 Stockholm, Sweden*
[c]*Department of Biosciences, University of Oslo, 0371 Oslo, Norway*

†Electronic supplementary information (ESI) available. See DOI: 10.1039/c8nr05598j

‡Current address: Center for Free-Electron Laser Science, University of Hamburg, 22761 Hamburg, Germany.
§Current address: RISE Bioeconomy, Box 5604, 114 86 Stockholm, Sweden.
¶Current address: Physics and Materials Science Research Unit, University of Luxembourg, 1511 Luxembourg, Luxembourg.

without the presence of a solid substrate. Here, we have quantified the nanoscale assembly of cellulose nanocrystals in an acoustically levitating drop by time-resolved small angle X-ray scattering (SAXS). The volume change of the surfactant-free drop was continuously monitored as the water evaporated, and we probed the structural features of CNC dispersions from 1 vol% to ~38 vol%, which is significantly higher than previous studies have investigated. The changes in scaling of the separation distance as a function of particle concentration were related to the transition of CNC dispersions from an isotropic phase to a compressed nematic state and the effect of gelation.

Results and discussion

We have followed the evaporation-induced assembly of CNC in aqueous levitating drops using *in situ* SAXS. Fig. 1a shows a schematic illustration of the experimental set-up, where the levitating drop was confined between two pressure nodes of an ultrasonic wave. The shrinkage of the drop was recorded using a USB camera (Fig. 1a), and the drop volume and particle concentration were estimated from the measured equatorial and polar radius (Fig. 1b). The CNC drop displayed a constant water evaporation rate of $\sim 10 \times 10^{-4}$ mm^3 s^{-1} until ~1000 s (Fig. S1†), where the evaporation rate decreased. Hindered water evaporation of CNC dispersions was recently studied and related to the formation of a particle network.[31–33] Fig. 1c shows representative SAXS curves of the shrinking CNC drop, which covered a particle concentration range from 1.5 vol% to 25 vol% (referring to the top and bottom curves, respectively). The growth of the primary peak in the SAXS curves is directly related to the time-dependent shrinkage of the drop and thus the increase of CNC concentrations. The primary scattering peak is related to the center-to-center separation distance ($d = 2\pi/q_{\text{peak center}}$, q is the scattering vector) between neighbouring particles.[16] The shift of the scattering peak towards higher q with increasing particle concentrations in Fig. 1c indicates a decreasing proximity between CNC particles, which is also observed in the development of the structure factors with increasing particle concentrations (Fig. S2†). The scattering curves also displayed a secondary peak, which previously has been related to the formation of anisotropic 2-dimensional CNC aggregates.[34]

The structural features of the CNC dispersion in a levitating drop with an initial diameter of ~1.5 mm was analyzed by power law scaling of the separation distance with CNC concentration. Fig. 2 shows that the separation distance continuously

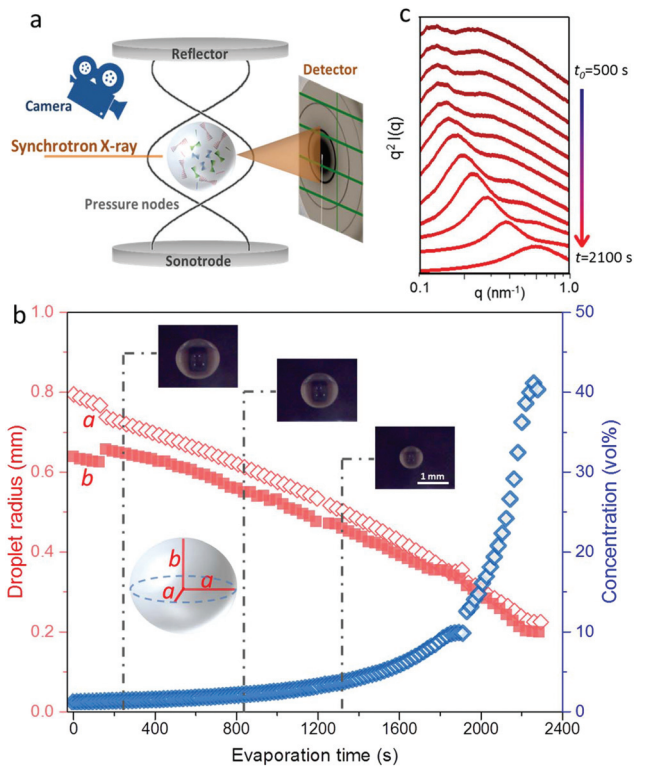

Fig. 1 Scheme of the experimental set-up, the evolution of drop dimension and concentration and representative SAXS curves. (a) Illustration of a levitating CNC drop between two pressure nodes of an ultrasonic wave that is illuminated by an incident X-ray beam. (b) Change of the drop dimension [equatorial (*a*) and polar (*b*) radius, respectively] and calculated CNC concentrations as a function of the evaporation time. The fluctuation around 200 s and 1900 s is due to a momentary oscillation of the drop. The inset images show the shrinkage of the CNC drop. (c) Representative Kratky plots of the time-resolved SAXS data of the shrinking drop. The time lapse, Δt, between each SAXS profile is 145 s.

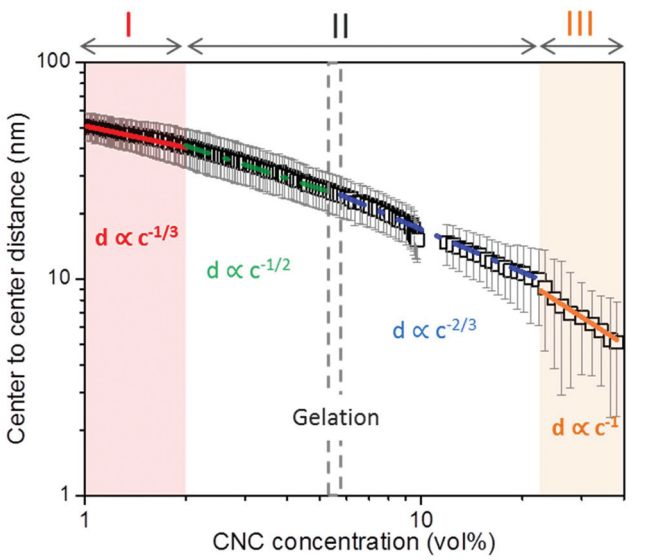

Fig. 2 Center-to-center separation distance (d) between CNC particles as a function of the particle concentration (c). The error bar results from the standard deviation of the fitted Gaussian peaks. The solid curves describe a power law relation ($d \propto c^{-x}$) with exponents of; 1/3 (red); 1/2 (green); 2/3 (blue) and 1 (orange), respectively, dividing the CNC assembly process into 3 sequential stages. All the fitting show an adjusted R-square value above 0.98 (see fitting details in Fig. S4†). The gelation threshold around 6 vol% of the CNC dispersions was determined from the gravity-driven flowing ability in tilted vials.

decreased from 50 nm to 5 nm as the CNC concentration increased from 1 vol% to more than 35 vol%. The reproducibility of the retrieved concentration-dependent separation distances from the SAXS measurements was confirmed by a repeated measurement on the other levitating drops with the same initial CNC concentration, as shown in Fig. S3.†

The scaling of the CNC dispersion at low concentrations (between 1 vol% and 2 vol%) followed $d \propto c^{-1/3}$ (Fig. 2, Stage I), which is characteristic for isotropic contraction of randomly aligned particles. Indeed, this concentration range coincided with the isotropic state of the CNC dispersion, as shown in the phase diagram of Fig. S5a.†[16] The isotropic state is also confirmed by the absence of any birefringent regions when the dispersion was placed between crossed polarizers (Fig. S6†). The scaling for unidimensional compression of the nematic phase ($d \propto c^{-1}$) was obtained only at very high concentrations (above 23 vol%, Stage III). Hence, there is a significant concentration range (between 2 and 23 vol%) where the structural change of CNC drop displayed transitional scaling exponents from −1/3 to −1. At particle concentrations above 2 vol% up to ~6 vol%, the CNC dispersion followed a scaling of $d \propto c^{-1/2}$. The concentration dependence of the separation distance in the levitating CNC drops within this concentration range was in good agreement with the previous study of Schütz *et al.* (Fig. S5b†),[16] where biphasic CNC dispersions with concentrations between 1.9 vol% and 5.2 vol% were measured in sealed capillaries (near equilibrium conditions) by SAXS. The close correspondence in scaling behavior of these two data sets suggests that the geometrical constraints of the relatively large levitating drop (with a diameter between 1.2 mm to 0.8 mm) have an insignificant influence on the structural evolution of CNC assembly,[21,22] and thus implies that the power law scaling of $d \propto c^{-1/2}$ is characteristic for the biphasic state of bulk CNC dispersions. In addition, no characteristic peaks of a hexagonal packing structure (expected peak position ratio of $1 : \sqrt{3} : 2$) were observed in Fig. 1c,[35–37] which indicates that the scaling power of −1/2 excludes the packing of the CNC particles into a hexagonal lattice.

Chiral nematic assembly of CNC is always accompanied and competing with gelation at high concentrations (above 6–9 vol%).[3,19,38] The competition between gelation and self-assembly is still poorly understood, but of significance for producing CNC-based materials with controllable helical orientation and chiral nematic pitch.[3,19] Investigation of the gravity-driven flowing ability of CNC dispersions in tilted vials at different concentrations suggests that the gelation threshold of CNC used in this study was around 6 vol% (Fig. S7†). It is interesting to note that a change of the scaling relation from $d \propto c^{-1/2}$ to $d \propto c^{-2/3}$ occurred at a CNC concentration of 6 vol%, which indicates that the scaling of $d \propto c^{-2/3}$ may reflect the competition between gelation and unidirectional compression of the fully nematic phase. Fig. S8† shows that the Porod invariant $Q \propto \bar{\rho} \cdot c \cdot (1 - c)$, where ρ and c are the average electron density difference between CNC and the solvent and CNC concentration, respectively,[39] increased until a maximum value is obtained around an evaporation time of ~2000 s, which corresponds to a CNC concentration of ~20 vol%. This particle concentration corresponds to the onset of the unidimensional compression, and the increase of the scattering power (*i.e.* the magnitude of Q) may thus reflect the fusion and rearrangement of the cholesteric tactoids in the viscoelastic dispersion, similar to a recent study using electron microscopy.[26] Fig. S9† shows that the order parameter (F) increases with increasing CNC concentrations and reaches a maximum value at a CNC

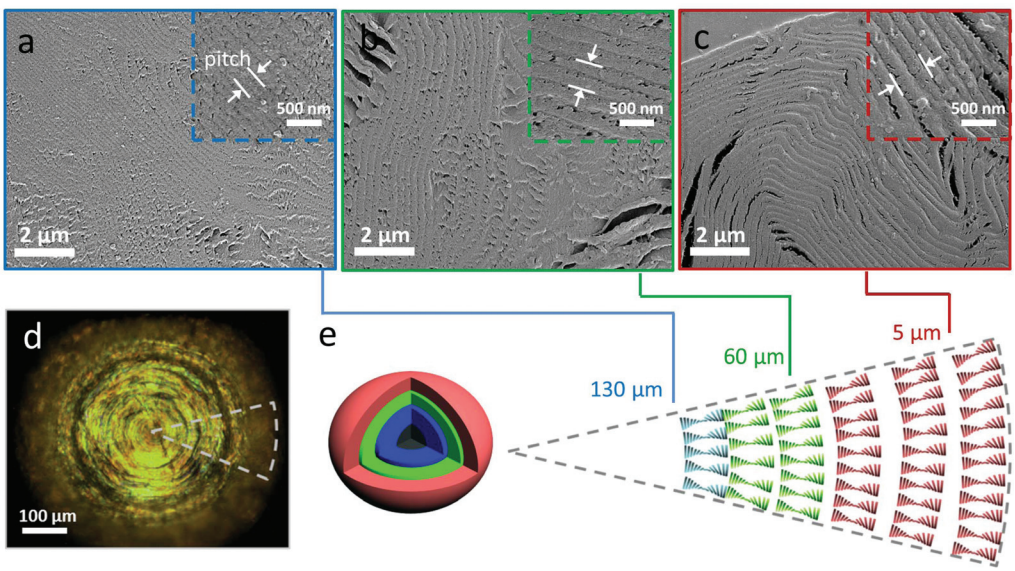

Fig. 3 Structural characterization of the dry CNC bead. Scanning electron microscopy (SEM) images of the cross-sectional surface in the; (a) core, (b) intermediate layer and (c) outer layer of the CNC bead with a distance from the bead surface of 5 μm, 60 μm and 130 μm, respectively. Inset images show a magnified view. The dry CNC bead was ultramicrotome-sectioned through the center. (d) Polarized optical microscopy image of the CNC bead (crossed polarizers). (e) Schematic illustration of the helicoidal structure within the dry bead.

concentration of ~20 vol%. The decrease of Q and F at higher particle concentrations (*i.e.*, longer evaporation time) is likely related to the formation of defects, cracks and possibly also voids, similar to previous findings in studies on assembly of iron oxide nanoparticles in levitating drops.[39] In addition, we have evaluated the ionic strength effect on the assembly of CNC. The separation distance was always larger than the corresponding Debye length (Fig. S10†), which suggests that agglomeration of CNC is of minor importance in this study.

The SEM images of the internal structure in Fig. 3a–c shows that the dry CNC bead displayed a layered microstructure, which is characteristic for the chiral nematic structure.[3,11,17] The chiral nematic structure of the CNC bead was further evidenced by the birefringent appearance under crossed polarizers. In contrast to previous studies on CNC assembled in small drops in surfactant-containing systems,[22,23] we did not observe any significant structural differences between the core (Fig. 3a) and outer shell (Fig. 3c) of the assembled bead beyond the pitch value. The helical pitch, measured on SEM micrographs (Fig. 3a–c) within the bead ranged from 410 ± 60 nm to 220 ± 30 nm from the outer layer to the core of the bead, which is significantly smaller than the pitch of CNC assembled in small, confined droplets (pitch of ~1.3 μm),[22] but similar to the pitch (~200 nm) observed in CNC films prepared by drop casting a dispersion on the substrate in Fig. S11.†

Conclusions

The structural evolution of CNC dispersions during evaporation have been quantified using a substrate-free levitating setup combined with SAXS, covering a very wide concentration range; from 1 vol% up to 38 vol%. The nanoscale assembly was evaluated by analyzing the scaling of the separation distance as a function of the particle concentration, and the scaling relations was related to the transition from an isotropic state to a compressed chiral nematic structure. Complemented by the phase diagram, a scaling relation of $d \propto c^{-1/2}$ from 2 vol% to 6 vol% was characteristic for the structural features of biphasic dispersions, while the change of scaling into $d \propto c^{-2/3}$ around 6 vol% correlated well with the gelation threshold of CNC. The dry CNC beads displayed chiral nematic structures of *e.g.*, similar pitch values compared to the casted planar CNC films. This study provides a quantitative tool to study assembly at very high particle concentrations in drops that are sufficiently large to resemble bulk systems, of relevance for fabricating CNC-based photonics.

Experimental section

Preparation and characterization of cellulose nanocrystals

CNC with an average length of 178 ± 76 nm and an average diameter of ~4 nm were fabricated using a sulfuric acid hydrolysis protocol.[16] The sulfate half-ester groups on the CNC surface provided a charge of 0.23 mmol g^{-1}, as determined by polyelectrolyte titration. The initial volume fraction of CNC, c_0, was calculated in the following equation:

$$c_0 = \frac{\rho_{\text{water}} \cdot \omega_{\text{CNC}}}{\rho_{\text{water}} \cdot \omega_{\text{CNC}} + \rho_{\text{CNC}} \cdot (1 - \omega_{\text{CNC}})}$$

where ρ is the density (1.6 g cm^{-3} and 1 g cm^{-3} for CNC and water, respectively),[9] ω_{CNC} the CNC mass fraction (1 wt%).

Drop levitation

Generally, a 1.5–3 μL drop of aqueous CNC dispersions (1 vol%) was placed into the acoustic field of the levitator (TEC5, model 13K11, f_0 = 100 kHz) where the drop was stabilized by adjusting the distance between the reflector and transducer, as well as the acoustic power. The acoustic levitator was encapsulated in a glass chamber with four opening sides, for the X-ray beam going through and a USB camera (1.3 M pixels, magnification up to 200×) recording, respectively. Image J and Origin 2015 were used to analyze the shrinkage of drop volume, and the average particle concentration as a function of the evaporation time was calculated using following equations:

$$V_{\text{drop}}(t) = 4/3\pi a^2 b$$

$$V_{\text{CNC}} = c_0 V_{0,\text{drop}}$$

$$c(t) = V_{\text{CNC}}/V_{\text{drop}}(t)$$

where t is the evaporation time, V the volume, a the equatorial radius and b the polar radius of the levitating drop.

Small angle X-ray scattering

SAXS experiments were performed on the beamline I911-4 at MAX-lab, Sweden. The beamline applies a multipole wiggler where the Si (111) monochromator provides X-ray with a wavelength of 0.91 Å. The beam size was 0.2 × 0.3 mm^2. A hybrid pixel CCD detector Pilatus 1 M (pixel size 172.0 μm) was used to obtain the 2-dimensional SAXS patterns and the distance from the sample to the detector was set to 1921.8 mm after calibration with silver behenate. The exposure time for each measurement was 10 s. The background scattering of deionized water was subtracted prior to the radial integration using bli9114.[40] The scattering intensity $I(q)$ of CNC dispersions reflects a combination of form factor $P(q)$ and structure factor $S(q)$.

$$S(q) = \frac{I(q)}{P(q)}$$

$P(q)$ solely depends on the shape and dimension of CNC particles, while $S(q)$ reflects how the nanoparticles are arranged with respect to each other. The structural peaks in the SAXS curves were Gaussian fitted and used to determine an average center-to-center particle separation distance by the equation:

$$d = \frac{2\pi}{q_{\text{peak center}}}$$

where $q_{\text{peak center}}$ is the scattering vector at the peak center.

Porod invariant calculation

The Porod invariant, Q, of CNC drops during evaporation was calculated by the equation:

$$Q = \int_{q_{\min}}^{q_{\max}} I(q) q^2 \mathrm{d}q$$

where I (q) is the scattering intensity and q the scattering vector.

Order parameter calculation

The scattering intensity was plotted as a function of azimuthal angles along the crystalline cellulose (200), and the full width at half (FWHM) was obtained by Gaussian peak fitting. The order parameter, F, is calculated by the equation:

$$F = \frac{180 - \mathrm{FWHM}}{180}$$

Scanning electron microscopy

CNC bead was mounted on a silver pin using epoxy resin (Epoxy embedding medium, Fluka) and sectioned using ultra-microtome Leica EMFC7 equipped with a diamond knife (Diatome). The sample was sputter coated with a thin layer of platinum (Cressington 308R). The cross-sectional surface of CNC beads was characterized by scanning electron microscope (Hitachi S-4800).

Polarized optical microscopy

The polarized optical image of the CNC bead was taken in the reflection mode of a Nikon Eclipse FNI light microscope and then recorded by an inline camera with a CCD sensor (2 M pixels).

Calculation of Debye length

The Debye length, κ^{-1}, was calculated using the following formula:

$$\kappa^{-1} = \sqrt{\frac{\varepsilon_r \varepsilon_o k_B T}{2 N_A e^2 I}}$$

where ε_r is the dielectric constant, ε_o the permittivity of free space, k_B the Boltzmann constant, T the temperature in Kelvin, N_A the Avogadro number, e the elementary charge and I the ionic strength.

Conflicts of interest

There are no conflicts to declare.

Acknowledgements

We acknowledge the Wallenberg Wood Science Center and the Swedish Research Council (VR) for funding. Thanks are given to MAX IV for the synchrotron beam time under the proposal (20130343 and 20140492) and the levitator. Ana Labrador and Tomás S. Plivelic are acknowledged for the technical assistance. We thank Bruno Frka-Petesic, Oliver Willekens, Daniela Stoeckel and Wim Thielemans for useful discussions. CS thanks the Alexander von Humboldt Foundation for funding under the Feodor Lynen scholarship.

Notes and references

1 L. Bergström, E. V. Sturm née Rosseeva, G. Salazar-Alvarez and H. Cölfen, *Acc. Chem. Res.*, 2015, **48**, 1391–1402.
2 P. Fratzl, *J. R. Soc., Interface*, 2007, **4**, 637–642.
3 J. P. F. Lagerwall, C. Schütz, M. Salajkova, J. Noh, J. Hyun Park, G. Scalia and L. Bergström, *NPG Asia Mater.*, 2014, **6**, e80.
4 J. C. Weaver, G. W. Milliron, A. Miserez, K. Evans-Lutterodt, S. Herrera, I. Gallana, W. J. Mershon, B. Swanson, P. Zavattieri, E. DiMasi and D. Kisailus, *Science*, 2012, **336**, 1275–1280.
5 T. Wang, D. LaMontagne, J. Lynch, J. Zhuang and Y. C. Cao, *Chem. Soc. Rev.*, 2013, **42**, 2804–2823.
6 B. Wicklein, A. Kocjan, G. Salazar-Alvarez, F. Carosio, G. Camino, M. Antonietti and L. Bergström, *Nat. Nanotechnol.*, 2015, **10**, 277–283.
7 F. G. Omenetto and D. L. Kaplan, *Science*, 2010, **329**, 528–531.
8 A. R. Studart, *Adv. Mater.*, 2012, **24**, 5024–5044.
9 R. J. Moon, A. Martini, J. Nairn, J. Simonsen and J. Youngblood, *Chem. Soc. Rev.*, 2011, **40**, 3941–3994.
10 J. F. Revol, H. Bradford, J. Giasson, R. H. Marchessault and D. G. Gray, *Int. J. Biol. Macromol.*, 1992, **14**, 170–172.
11 J. F. Revol and R. H. Marchessault, *Int. J. Biol. Macromol.*, 1993, **15**, 329–335.
12 M. Eder, K. Jungnikl and I. Burgert, *Trees*, 2009, **23**, 79–84.
13 S. Vignolini, P. J. Rudall, A. V. Rowland, A. Reed, E. Moyroud, R. B. Faden, J. J. Baumberg, B. J. Glover and U. Steiner, *Proc. Natl. Acad. Sci. U. S. A.*, 2012, **109**, 15712–15715.
14 R. M. Graham, D. W. Lee and K. Norstog, *Am. J. Bot.*, 1993, **80**, 198–203.
15 O. D. Onelli, T. van de Kamp, J. N. Skepper, J. Powell, T. S. dos Rolo, T. Baumbach and S. Vignolini, *Sci. Rep.*, 2017, **7**, 1373.
16 C. Schütz, M. Agthe, A. B. Fall, K. Gordeyeva, V. Guccini, M. Salajková, T. S. Plivelic, J. P. F. Lagerwall, G. Salazar-Alvarez and L. Bergström, *Langmuir*, 2015, **31**, 6507–6513.
17 J. H. Park, J. Noh, C. Schütz, G. Salazar-Alvarez, G. Scalia, L. Bergström and J. P. F. Lagerwall, *ChemPhysChem*, 2014, **15**, 1477–1484.
18 M. Giese, L. K. Blusch, M. K. Khan and M. J. MacLachlan, *Angew. Chem., Int. Ed.*, 2015, **54**, 2888–2910.
19 R. M. Parker, G. Guidetti, C. A. Williams, T. Zhao, A. Narkevicius, S. Vignolini and B. Frka-Petesic, *Adv. Mater.*, 2017, 1704477.

20 Y. Liu, D. Stoeckel, K. Gordeyeva, M. Agthe, C. Schütz, A. B. Fall and L. Bergström, *ACS Macro Lett.*, 2018, **7**, 172–177.
21 Y. Li, J. Jun-Yan Suen, E. Prince, E. M. Larin, A. Klinkova, H. Thérien-Aubin, S. Zhu, B. Yang, A. S. Helmy, O. D. Lavrentovich and E. Kumacheva, *Nat. Commun.*, 2016, **7**, 12520.
22 R. M. Parker, B. Frka-Petesic, G. Guidetti, G. Kamita, G. Consani, C. Abell and S. Vignolini, *ACS Nano*, 2016, **10**, 8443–8449.
23 P. X. Wang, W. Y. Hamad and M. J. MacLachlan, *Angew. Chem., Int. Ed.*, 2016, **55**, 12460–12464.
24 X. M. Dong, J. F. Revol and D. G. Gray, *Cellulose*, 1998, **5**, 19–32.
25 X. M. Dong, T. Kimura, J. F. Revol and D. G. Gray, *Langmuir*, 1996, **12**, 2076–2082.
26 P. X. Wang, W. Y. Hamad and M. J. MacLachlan, *Nat. Commun.*, 2016, **7**, 11515.
27 P. X. Wang and M. J. MacLachlan, *Philos. Trans. R. Soc., A*, 2018, **376**, 20170042.
28 A. M. Seddon, S. J. Richardson, K. Rastogi, T. S. Plivelic, A. M. Squires and C. Pfrang, *J. Phys. Chem. Lett.*, 2016, **7**, 1341–1345.
29 A. Omrane, S. Santesson, M. Alden and S. Nilsson, *Lab Chip*, 2004, **4**, 287–291.
30 J. Polte, F. Emmerling, M. Radtke, U. Reinholz, H. Riesemeier and A. F. Thünemann, *Langmuir*, 2010, **26**, 5889–5894.
31 F. Jativa, C. Schütz, L. Bergström, X. Zhang and B. Wicklein, *Soft Matter*, 2015, **11**, 5374–5380.
32 L. Pauchard and C. Allain, *C. R. Phys.*, 2003, **4**, 231–239.
33 R. Duggal, F. Hussain and M. Pasquali, *Adv. Mater.*, 2006, **18**, 29–34.
34 M. Uhlig, A. Fall, S. Wellert, M. Lehmann, S. Prévost, L. Wågberg, R. von Klitzing and G. Nyström, *Langmuir*, 2016, **32**, 442–450.
35 E. E. Maier, R. Krause, M. Deggelmann, M. Hagenbüchle, R. Weber and S. Fraden, *Macromolecules*, 1992, **25**, 1125–1133.
36 S. T. Hyde, *Langmuir*, 1997, **13**, 842–851.
37 E. Grelet and R. Rana, *Soft Matter*, 2016, **12**, 4621–4627.
38 D. G. Gray, *Philos. Trans. R. Soc., A*, 2018, **376**, 20170038.
39 M. Agthe, T. S. Plivelic, A. Labrador, L. Bergström and G. Salazar-Alvarez, *Nano Lett.*, 2016, **16**, 6838–6843.
40 A. Labrador, Y. Cerenius, C. Svensson, K. Theodor and T. Plivelic, *J. Phys.: Conf. Ser.*, 2013, **425**, 072019.